

Spectral link of the generalized Townsend-Perry constants in turbulent boundary layers

Björn Birnir¹, Luiza Angheluta², John Kaminsky¹, Xi Chen³

¹ CNLS and Department of Mathematics, University of California in Santa Barbara, USA

² The Njord Centre, Department of Physics, University of Oslo, P. O. Box 1048, 0316 Oslo, Norway

³ Institute of Fluid Mechanics, Beihang University, Beijing, China

We propose a minimal spectral theory for boundary layer turbulence that captures very well the profile of the mean square velocity fluctuations in the stream-wise direction, and gives a quantitative prediction of the Townsend-Perry constants. The phenomenological model is based on connecting the statistics in the streamwise direction with the energy spectrum of the streamwise velocity fluctuations. The original spectral theory was proposed in Ref. [8] to explain the friction factor and von Kármán law in Ref. [7]. We generalized it by including fluctuations in the wall-shear stress and the streamwise velocity. The predicted profiles for the mean velocity and mean square fluctuations are compared with velocity data from wind tunnel experiments.

I. INTRODUCTION

Turbulence is a ubiquitous phenomenon encountered in very diverse natural systems, from the large-scale atmosphere [27] and oceans [23] all the way down to quantum fluids [26], as well as in engineered systems, such as pipelines, heat exchangers, wind turbines, etc. It relates to the complex fluid dynamics that orchestrates the interactions of flow eddies spanning many length-scales and generating non-Gaussian statistics of velocity increments. The statistical properties of these turbulent fluctuations are fundamentally changed when the flow is confined by the presence of solid walls or boundaries [9, 22]. In contrast to bulk turbulence, which is statistically homogeneous and isotropic, the wall-bounded turbulence is characterised by statistically anisotropic properties. Namely, there is a net mean-flow in the streamwise direction along the wall and the different flow structures form depending on their distance to the wall. We typically differentiate between four flow regions as moving away from the wall [17]: i) the *viscous region* closest to the wall and where viscous flows dominate, ii) the *buffer layer*, marking the transition from the viscous layer into the inertial layer, iii) the *inertial layer* where the log-law of the wall applies, and iv) the *wake*, the energetic region beyond the inertial layer. A more refined division is given in [6].

A classical signature of wall-bounded turbulence is the "log-law of the wall" of the mean velocity profile (MVP) due to Prandtl and von Kármán, and reads as

$$\langle \tilde{u} \rangle = \frac{1}{\kappa} \log(\tilde{y}) + B, \quad (1)$$

where κ is the *universal* von Kármán constant that is independent of the microscopic flow characteristics and relates to generic features such as space dimensionality. The distance to the wall y and the mean fluid velocity u along the wall, are typically expressed in the "wall units" determined by the wall shear stress τ_0 . This is because τ_0 is an important theoretical concept that is also experimentally measurable. The friction velocity $u_\tau = \sqrt{\langle \tau_0 \rangle / \rho}$ which is set by the wall shear stress τ_0 and the kinematic

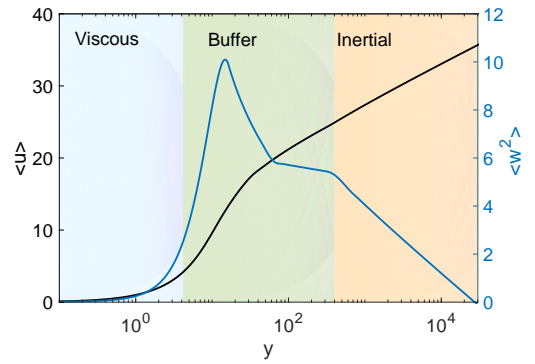


FIG. 1. Theoretical predictions from the spectral theory for the MVP $\langle u \rangle$ and mean square velocity fluctuations $\langle w^2 \rangle$ (dimensionless variables in wall units).

viscosity ν , and enters in the unit rescalings as $\tilde{u} = u/u_\tau$ and $\tilde{y} = yu_\tau/\nu$. The constant fluid density is ρ and the B is a dimensionless constant that is fitted to experimental data, e.g. [20].

A log-law of the wall was also derived from the "attached eddy hypothesis" by Townsend [24]. Townsend showed that the velocity fluctuations, $\tilde{w} = w/u_\tau$, $\tilde{u} = \langle \tilde{u} \rangle + \tilde{w}$, also follow the log-law of the wall in its second moment, namely

$$\langle \tilde{w}^2 \rangle = -A_1 \log(\tilde{y}) + B_1, \quad (2)$$

where the coefficients A_1 and B_1 , also called the Townsend-Perry constants, were first measured by Perry and Chong [18, 19].

More recently, the log-law was generalised to any moment of the streamwise velocity fluctuations, \tilde{w} , assuming Gaussian velocity fluctuations [15],

$$\langle \tilde{w}^{2p} \rangle^{1/p} = -A_p \log(\tilde{y}) + B_p. \quad (3)$$

While the generalised log-law is supported by wall-turbulence experiments, the dependance of A_p and B_p on p turns out to be sub-Gaussian, which is confirmed both

experimentally and numerically, [15]. The sub-Gaussian behavior was explained in Ref. [4] using the stochastic closure theory of turbulence [2, 3] and the analysis was improved in Ref. [12], using measurements from the Flow Physics Facility (FPF) at the University of New Hampshire. Both of these studies used the results from homogeneous turbulence [11] and made an assumption about the form of the fluctuating shear stress in the inertial layer, based on physical principles.

In Ref. [7], a spectral theory for the log-law of the wall of the MVP was proposed in which it is possible to derive the log-law in the inertial layer and the laminar profile in the viscous layer. The novel contribution is the precise form of the transition in the buffer layer using the Kolmogorov-Obukhov energy spectrum of turbulent fluctuations. The form of the MVP in the wake is also obtained. This was done by summing the energy of the wall-attached eddies, as hypothesised originally by Townsend in [24].

In this paper, we propose a generalisation of the spectral theory that includes fluctuations in the streamwise velocity due to an essentially fluctuating wall shear stress. Fig. 5 shows the spectral theory predictions of the profiles of the mean velocity and mean square velocity fluctuations across the viscous, buffer and inertial layers. The rest of the paper is structured as follow. We summarise the analysis in Ref. [7] and its extension in Section II, and generalise it to include the fluctuations in Section III. This produces the log law of the wall in Eq. (2) for the velocity fluctuations and its higher moments in Eq. (3). Then in Section IV, we derive the functional form of the mean-square fluctuations in the viscous layer and the inertial layer. In Section V, we use the attached eddy hypothesis and the stochastic closure theory [2, 3] to derive the form of the Townsend-Perry and the generalized Townsend-Perry constants. This allows us to derive the streamwise fluctuations in the wall shear stress, and remove the assumption made in Refs. [4] and [12], and mentioned above. Using theory-informed by data analysis, we can construct the Townsend-Perry constants and the generalised Townsend-Perry constants. In Section VI, we extend the formulas for the mean square fluctuations to the buffer layer and the energetic wake. In Section VII, we compare the predicted MVP and mean-square velocity profile from this spectral theory to experimental data. In Section VIII, we conclude with a discussion on the proposed spectral theory and the role that Townsend's attached eddies play in it.

II. THE SPECTRAL THEORY

The typical velocity of an inertial eddy of size s can be obtained by integrating out the kinetic energy contained in all eddies of sizes up to s as in Ref. [7]

$$v_s^2 = \int_{1/s}^{\infty} E(k) dk, \quad (4)$$

where kinetic energy spectrum follows the Kolmogorov-Obukhov scaling with cutoffs in the injection scale and viscous scales, $E(k) = c_d(\eta k)^{2/3}(\kappa_\epsilon \epsilon)^{2/3} k^{-5/3} c_e(Rk)$, with $\frac{2}{3}(\kappa_\epsilon \epsilon)^{2/3} k^{-5/3}$ being the Kolmogorov-Obukhov spectrum and $c_d(\eta k)$ and $c_e(Rk)$ the phenomenological dimensionless corrections functions in the dissipative (set by the Kolmogorov scale η) and energetic range (set by the system size R), respectively. κ_ϵ is a dimensionless parameter, ϵ is the turbulent energy dissipation rate, $\eta = \nu^{3/4} \epsilon^{-1/4}$ is the viscous length scale and R is the largest length scale in the flow. The dissipative correction function is typically an exponential cutoff function $c_d(\eta k) = \exp(-\beta_d \eta k)$, and the energetic-range (wake) correction function is $c_e(Rk) = (1 + (\beta_e/(Rk))^2)^{-17/4}$, which is the form that was proposed by von Kármán. β_d and β_e are non-negative fitting parameters that can be adjusted to data. By the change of variables $\xi = sk$, we recast Eq. (4) as

$$v_s^2 = (\kappa_\epsilon \epsilon s)^{2/3} I\left(\frac{\eta}{s}, \frac{s}{R}\right), \quad (5)$$

where the spectral function I is given by the formula [7]

$$I\left(\frac{\eta}{s}, \frac{s}{R}\right) = \frac{2}{3} \int_1^{\infty} e^{-\xi \beta_d \eta/s} \xi^{-5/3} \left(1 + \left(\frac{\beta_e s}{R\xi}\right)^2\right)^{-17/6} d\xi. \quad (6)$$

The integral sums the energies of all eddies of a smaller radius than s , and computes their contribution to the energy of the eddy of radius s . This is the energy (or spectral) formulation of the attached eddy hypothesis of Townsend [24]. The I -function correctly captures the buffer layer, as the transition from the viscous to the inertial layer, and the asymptotic of the MVP in the energetic wake. The asymptotic values are such that in the inertial layer $I = 1$ and in the viscous layer $I = 0$. The I -function combines the Kolmogorov-Obukhov theory with the observed spectrum in the viscous layer, the inertial layer and the wake and is thus able to capture the transition from one layer to the next. In Ref [7], it was used to give the details of the MVP. In this paper, we will use it to capture the profile of mean-square fluctuations.

In the buffer layer a different scaling of the attached eddies comes into play, this is the k_x^{-1} scaling of the spectrum that has been debated in literature, but clearly shows up in recent simulations and experiments in the middle of the buffer layer, see Figure 9 (a) in Ref. [14] and Figure 12 (b) in Ref. [21]. In the spectral theory, corresponding I -function for this scaling regime is

$$I_b\left(\frac{\eta}{s}, \frac{s}{R}\right) = \frac{2}{3} s^{-2/3} \int_1^{\infty} e^{-\xi \beta_d \frac{\eta}{s}} \xi^{-1} \left(1 + \left(\frac{\beta_e s}{R\xi}\right)^2\right)^{-17/6} d\xi, \quad (7)$$

where the subscript b stands for "buffer". The mean velocity is primarily influenced by the I -function, whereas

the variation (fluctuation squared) is greatly influenced by the I_b -function in the buffer layer. I is associated with the Kolmogorov-Obukhov energy cascade $k_x^{-5/3}$, in the inertial layer, whereas I_b is associated with the k_x^{-1} scaling in the buffer layer. (Here the x denotes the stream-wise direction.) We will take I_b to be zero outside the buffer layer.

The splitting of the near-wall region based on different scaling of the spectrum was proposed by Perry and Chong [18] who used it to build an interpolation model for MVP and the variation, this model was improved in Ref. [25].

III. THE GENERALISED LOG-LAW

In this section, we will give a simple derivation of the log-law for the mean-square velocity profile that holds in the limit of large Reynolds number. In the following section we derive the general form of the variation that is not equally transparent.

We will generalize the derivation of the MVP in Ref. [7], by adding a fluctuation to the mean velocity. We let the velocity along the wall be

$$v_1 = u + v_1 - u = u + w, \quad (8)$$

where u is the mean velocity obtained by averaging v_1 over time, and w is the fluctuation. The same derivations as in Ref. [7] give the following equations for a dominant eddy of radius $s = y$, if we include the velocity fluctuations. In Ref. [7] the shear stress at the distance y from the wall is given by the formula $\bar{\tau}_t = \kappa_\tau \rho y v_y u'$ where u' denotes the y derivative of the velocity u along the wall, and the overline indicates a not-fluctuating quantity. When velocity fluctuations are included the shear stress becomes:

$$\tau_t = \kappa_\tau \rho y v_y (u' + w'), \quad (9)$$

where ρ is the density v_y is the (rotational) velocity of an eddy a distance y from the wall and κ_τ is the dimensionless proportionality factor. The energy dissipation rate is related to the wall shear stress as $\bar{\epsilon} = \tau_t u' / \rho$ [7], and including the fluctuations, this becomes

$$\epsilon = \tau_t (u' + w') / \rho. \quad (10)$$

The eddy velocity for an eddy with radius $s = y$ at the distance y from the wall is the same as in Ref. [7], and as discussed above,

$$v_y = (\kappa_\epsilon \epsilon y)^{1/3} \sqrt{I}, \quad (11)$$

where I is the integral from Eq. (6) and κ_ϵ is a dimensionless proportionality factor. In the inertial layer $I = 1$ and $\kappa_\epsilon = 4/5$ according to Kolmogorov's 4/5 law.

Eliminating ϵ and v_y from the three equations above, we obtain

$$\tau_t = (\kappa_\epsilon \kappa_\tau^3)^{1/2} \rho y^2 (u' + w')^2 I^{3/4}. \quad (12)$$

The viscous shear stress is $\rho \nu (u' + w')$ so the total shear stress, including the contribution from the fluctuation is [24]

$$\tau_t + \rho \nu (u' + w') = \tau_0 (1 - y/R). \quad (13)$$

Our assumption is that the wall shear stress τ_0 is also a quantity that fluctuates about its mean value.

We change the rescaled variables in the wall units written here in terms of the friction factor f : $\tilde{y} = y Re \sqrt{f} / R$, $\tilde{u} = u / (U \sqrt{f})$ and $\tilde{w} = w / (U \sqrt{f})$ and let $f = \langle \tau_0 \rangle / \rho U^2$. Then, the equation above becomes

$$\tilde{\kappa}^2 \tilde{y}^2 (\tilde{u}' + \tilde{w}')^2 I^{3/4} + (\tilde{u}' + \tilde{w}') = \frac{\tau_0}{\langle \tau_0 \rangle} \left(1 - \frac{\tilde{y}}{Re \sqrt{f}} \right). \quad (14)$$

If we let $\tilde{y} \rightarrow 0$, $\tilde{w} \rightarrow 0$ and integrate, we get the law of the viscous layer

$$\tilde{u} = \tilde{y}, \quad (15)$$

the laminar profile being

$$\tilde{u} = \left(\tilde{y} - \frac{\tilde{y}^2}{2 Re \sqrt{f}} \right). \quad (16)$$

In the large Reynolds number limit, solving just for the mean velocity, we obtain the Prandtl-von Kármán law

$$\tilde{u} = \frac{1}{\tilde{\kappa}} \log(\tilde{y}) + D. \quad (17)$$

This is the correct leading term but the full formulas in the next section are more complicated. We now motivate the log-law for the variation. If we solve for both the mean velocity and the fluctuation in the large Reynolds number limit, we get that

$$\tilde{u} + \tilde{w} = \frac{\sqrt{\tau_0}}{\langle \tau_0 \rangle^{1/2} \tilde{\kappa}} \log(\tilde{y}) + C. \quad (18)$$

This is consistent with the Eq. (17) in the sense that if $\sqrt{\tau_0} = \langle \tau_0 \rangle^{1/2}$, then $\tilde{w} = 0$ and we recover Eq. (17). Thus squaring Eq. (18) gives that

$$\tilde{u}^2 + 2\tilde{u}\tilde{w} + \tilde{w}^2 = \frac{\tau_0}{\langle \tau_0 \rangle \tilde{\kappa}^2} (\log(\tilde{y}))^2 + 2 \frac{\sqrt{\tau_0}}{\tilde{\kappa} \sqrt{\langle \tau_0 \rangle}} C \log(\tilde{y}) + C^2. \quad (19)$$

Taking the average, using that $\langle \tilde{w} \rangle = 0$ and Eq. (17), we get that

$$\langle \tilde{w}^2 \rangle = \frac{2C \langle \sqrt{\tau_0} \rangle - 2D \sqrt{\langle \tau_0 \rangle}}{\tilde{\kappa} \sqrt{\langle \tau_0 \rangle}} \log(\tilde{y}) + C^2 - D^2. \quad (20)$$

By comparing this with the generalised log-law in Eq. (2), for the fluctuations squared, we obtain

$$\langle \tilde{w}^2 \rangle = -A \log(\tilde{y}) + B, \quad (21)$$

where $A = -\frac{2C \langle \sqrt{\tau_0} \rangle - 2D \sqrt{\langle \tau_0 \rangle}}{\tilde{\kappa} \sqrt{\langle \tau_0 \rangle}}$ and $B = C^2 - D^2$ are the Townsend-Perry constants. The full formulas in next

section show that Eq. (21) is the leading term and $A = -2C \left(\frac{\langle \sqrt{\tau_0} \rangle - \sqrt{\langle \tau_0 \rangle}}{\kappa \sqrt{\langle \tau_0 \rangle}} \right)$, with $C = D$.

To simplify the notation, we will now drop the tilde's from all the variable with the dimensionless units implicitly assumed, unless otherwise stated.

IV. THE FUNCTIONAL FORM OF THE TOWNSEND-PERRY LAW

We will now use Eq. (14) to find the general form of the average of the fluctuations squared as a function of the distance to the wall. We consider the Eq. (14)

$$\kappa^2 y^2 (u' + w')^2 I^{3/4} + (u' + w') = \frac{\tau_0}{\langle \tau_0 \rangle} \left(1 - \frac{y}{Re\sqrt{f}} \right), \quad (22)$$

and first set $I = 0$ in the viscous layer. Then

$$u = y - \frac{y^2}{2Re\sqrt{f}} \quad (23)$$

by averaging and integration in y . Integrating Eq. (22) and subtracting u gives,

$$w = \frac{\tau_0 - \langle \tau_0 \rangle}{\langle \tau_0 \rangle} \left(y - \frac{y^2}{2Re\sqrt{f}} \right) \quad (24)$$

and

$$\langle w^2 \rangle = \frac{\langle \tau_0^2 \rangle - \langle \tau_0 \rangle^2}{\langle \tau_0 \rangle^2} \left(y - \frac{y^2}{2Re\sqrt{f}} \right)^2. \quad (25)$$

In the inertial layer $I = 1$ and ignoring the small $O(1/y^4)$ term, we get that

$$\begin{aligned} u + w = & \frac{1}{2\kappa^2 y} + 2 \frac{\sqrt{\tau_0}}{\kappa \sqrt{\langle \tau_0 \rangle}} \sqrt{1 - \frac{y}{2Re\sqrt{f}}} \\ & - 2 \frac{\sqrt{\tau_0}}{\kappa \sqrt{\langle \tau_0 \rangle}} \tanh^{-1} \left(\sqrt{1 - \frac{y}{2Re\sqrt{f}}} \right) + K, \end{aligned} \quad (26)$$

where K is a constant. Then setting $w = 0$, we get that

$$\begin{aligned} u = & \frac{1}{2\kappa^2 y} + \frac{2}{\kappa} \sqrt{1 - \frac{y}{2Re\sqrt{f}}} \\ & - \frac{2}{\kappa} \tanh^{-1} \left(\sqrt{1 - \frac{y}{2Re\sqrt{f}}} \right) + K', \end{aligned} \quad (27)$$

where K' is another constant, because τ_0 becomes $\langle \tau_0 \rangle$. Subtracting, u from $u + w$ we get

$$\begin{aligned} w = & 2 \frac{(\sqrt{\tau_0} - \sqrt{\langle \tau_0 \rangle})}{\kappa \sqrt{\langle \tau_0 \rangle}} \sqrt{1 - \frac{y}{2Re\sqrt{f}}} \\ & - 2 \frac{(\sqrt{\tau_0} - \sqrt{\langle \tau_0 \rangle})}{\kappa \sqrt{\langle \tau_0 \rangle}} \tanh^{-1} \left(\sqrt{1 - \frac{y}{2Re\sqrt{f}}} \right) + C, \end{aligned} \quad (28)$$

where $C = K - K'$. Squaring w and taking the average gives

$$\begin{aligned} \langle w^2 \rangle = & 4C \frac{(\langle \sqrt{\tau_0} \rangle - \sqrt{\langle \tau_0 \rangle})}{\kappa \sqrt{\langle \tau_0 \rangle}} \sqrt{1 - \frac{y}{2Re\sqrt{f}}} \\ & - 4C \frac{(\langle \sqrt{\tau_0} \rangle - \sqrt{\langle \tau_0 \rangle})}{\kappa \sqrt{\langle \tau_0 \rangle}} \tanh^{-1} \left(\sqrt{1 - \frac{y}{2Re\sqrt{f}}} \right) \\ & + 4 \left[\frac{2(\langle \tau_0 \rangle - \sqrt{\langle \tau_0 \rangle} \langle \sqrt{\tau_0} \rangle)}{\kappa^2 \langle \tau_0 \rangle} \left(1 - \frac{y}{2Re\sqrt{f}} \right) \right. \\ & - 2 \sqrt{1 - \frac{y}{2Re\sqrt{f}}} \tanh^{-1} \left(\sqrt{1 - \frac{y}{2Re\sqrt{f}}} \right) \\ & \left. + \left[\tanh^{-1} \left(\sqrt{1 - \frac{y}{2Re\sqrt{f}}} \right) \right]^2 \right] + C^2. \end{aligned} \quad (29)$$

From $\tanh^{-1}(x) = \frac{1}{2} \log\left(\frac{1+x}{1-x}\right)$, we see that the second term in the last formula is of leading order and we get that

$$\langle w^2 \rangle \sim 2C \frac{(\langle \sqrt{\tau_0} \rangle - \sqrt{\langle \tau_0 \rangle})}{\kappa \sqrt{\langle \tau_0 \rangle}} \log \left(\frac{y}{Re\sqrt{f}} \right) + h.o.t. \quad (30)$$

This agrees with the formula (21) above. For higher order moments $\langle w^{2p} \rangle^{1/p}$ the similar term, linear in \tanh^{-1} and multiplied by $2C$, is of leading order,

$$\langle w^{2p} \rangle^{1/p} \sim 2C \frac{(\langle (\sqrt{\tau_0} - \sqrt{\langle \tau_0 \rangle})^p \rangle)^{1/p}}{\kappa \sqrt{\langle \tau_0 \rangle}} \log \left(\frac{y}{Re\sqrt{f}} \right) + h.o.t. \quad (31)$$

These formulas establish the log dependance of the second moment of the fluctuations, with the Townsend-Perry constants, and the log dependence of the higher moments of the fluctuations, with the Generalized Townsend-Perry constants, and justify formulas Eq. (2) and Eq. (3). Together, Eq. (2) and Eq. (3) can be called the generalised log-law of the wall.

V. DERIVATION OF THE GENERALIZED TOWNSEND-PERRY CONSTANTS

We consider the dependence of the fluctuation w on the distance x along the wall, to understand the Townsend-Perry constants. So far we have only considered $w(y)$ as a function of the distance y from the wall, but $w(x, y)$ obviously depends on both variables x and y . If we consider the eddy depicted in Fig. 2, then we see that the difference in momentum in the x direction, across the eddy, is given by

$$\rho(w(x+s) - w(x-s)) \sim 2\rho s w_x, \quad (32)$$

for y fixed, where $w_x = \frac{d}{dx} w$.

This means that the total turbulent stress, across a vertical surface at x , denoted by a dotted line on Fig. 2 for an eddy of radius $s \sim y$, is

$$\tau_0 = \tau_t + \tau_x, \quad (33)$$

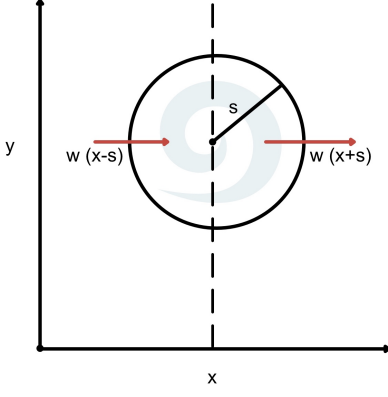


FIG. 2. The eddy of radius s and the variation in the fluctuations across it in the x (streamwise) direction.

where $\tau_x = 2\kappa_\tau \rho y w_x v_y$, analogous to formula Eq. (9) above. Then we get, using Eq. (11) and

$$\epsilon = (\tau_t + \tau_x)(u' + w_x)\rho, \quad (34)$$

that

$$\tau_t + \tau_x = \kappa^2 \rho I^{3/4} y^2 (u' + w_x)^2, \quad (35)$$

where prime denotes the derivative with respect to y , and

$$\begin{aligned} (\tau_t + \tau_x)^{1/2} &= \kappa \rho^{1/2} I^{3/8} y (u' + w_x) \\ &= \langle \tau_0 \rangle^{1/2} + \kappa \rho^{1/2} I^{3/8} y |w_x|, \end{aligned} \quad (36)$$

since both parts must be positive. The derivation is completely analogous to the derivation in Sec. III, but here with w varying in the x direction and $w_y = 0$. This gives that for y fixed,

$$\begin{aligned} \tau_0^{1/2} - \langle \tau_0 \rangle^{1/2} &= (\tau_t + \tau_x)^{1/2} - \langle \tau_0 \rangle^{1/2} \\ &= \kappa \rho^{1/2} I^{3/8} y |w_x|. \end{aligned} \quad (37)$$

Considering the leading order $\log(y/2Re\sqrt{f})$ term in Eq. (30) gives the Townsend-Perry constant

$$A_1 = \frac{2C\rho^{1/2}y\langle |w_x| \rangle}{\sqrt{\langle \tau_0 \rangle}}, \quad (38)$$

and the generalized Townsend-Perry constants

$$A_p = \frac{2C\rho^{1/2}y\langle |w_x|^p \rangle^{1/p}}{\sqrt{\langle \tau_0 \rangle}}, \quad (39)$$

by use of Eq. (31). This justifies the form of the stress tensor assumed in Ref. [4] and used in Ref. [12]. Finally, we get the expressions

$$A_1 = K\langle |w(x+y) - w(x-y)| \rangle \quad (40)$$

and

$$A_p = K\langle |w(x+y) - w(x-y)|^p \rangle^{1/p}, \quad (41)$$

where K is a constant and this produces the relationship between the Townsend-Perry and the generalized Townsend-Perry constants and the structure function of turbulence, see Ref. [2, 3, 11], used in Ref. [4, 12],

$$A_1 = KC_1|y^*|^{\zeta_1}, \quad (42)$$

$$A_2 = KC_2^{1/2}|y^*|^{\zeta_2/2}, \quad (43)$$

and

$$A_p = KC_p^{1/p}|y^*|^{\zeta_p/p}, \quad (44)$$

where $-y \leq y^* \leq y$. Considering the ratio, washes out the constant K ,

$$\frac{A_p}{A_2} = \frac{C_p^{1/p}}{C_2^{1/2}}|y^*|^{\zeta_p/p - \zeta_2/2}, \quad (45)$$

where the C_p s are the Kolmogorov-Obukhov coefficients of the structure functions from Ref. [2, 3, 11]. The last ratio was used in Ref. [12] to get agreement between experimental data and theory.

VI. THE SPECTRAL THEORY OF MEAN-SQUARE FLUCTUATIONS

In the above sections we have not used the spectral information in the integral I , in Eq. (6). We have just used the attached eddy hypothesis and set $I = 0$ in the viscous layer and $I = 1$ in the inertial layer. But following Ref. [7], we can now use the spectral information through the integral I to find the beginning of the buffer layer and the form of both the MVP u and the fluctuation w in the buffer layer and in the wake. This allows one to obtain the full functional form of both u and w as functions of the distance y from the wall and compare it with the experimental data in the next section. By use of the energy Eq. (10) and the relation $\eta = \nu^{3/4}\epsilon^{-1/4}$ we can find an expression for η/y , the viscosity parameter that increases as we approach the wall $y \rightarrow 0$. If we set the fluctuation equal to zero,

$$\eta/y = (\tilde{u}'(1 - \tilde{y}/Re\sqrt{f}) - (\tilde{u}')^2)^{-1/4}\tilde{y}^{-1} \quad (46)$$

and find a formula for \tilde{y} using this equation along with the equation

$$\kappa^2 \tilde{y}^2 (u')^2 I^{3/4} + u' = \frac{\tau_0}{\langle \tau_0 \rangle} \left(1 - \frac{y}{Re\sqrt{f}} \right). \quad (47)$$

The resulting formula is given in Ref. [7],

$$\tilde{y} = \left(\frac{(\eta/y)^{4/3} + \kappa^{4/3} I^{1/2} (\eta/y, 0)}{\kappa^{2/3} (\eta/y)^{8/3} I^{1/4} (\eta/y, 0)} \right). \quad (48)$$

It gives the minimum value of \tilde{y} for which $I(\eta/y, 0) > 0$ and the small eddies begin to contribute to the turbulent

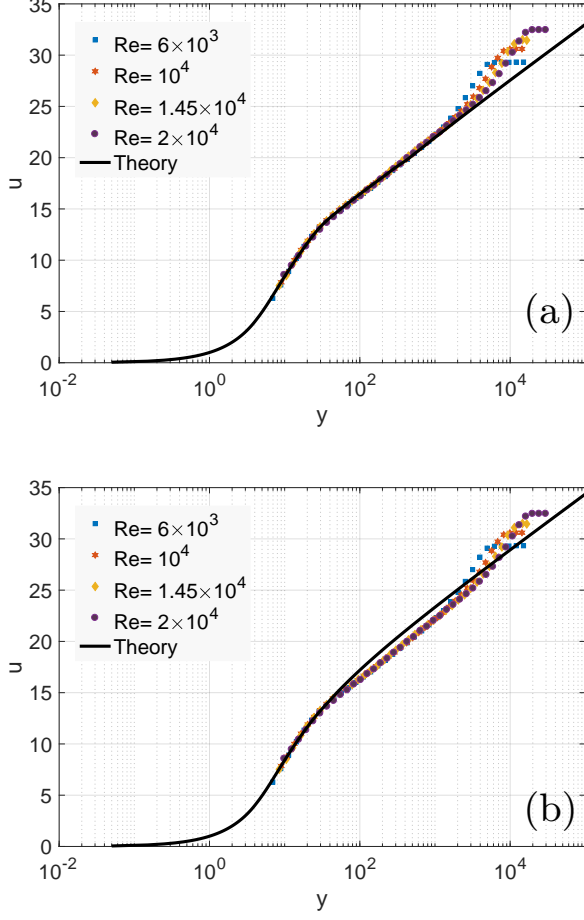


FIG. 3. The average of the MVP as a function of $\log(y)$, where y is the distance from the wall. Comparison of experimental data with theory (black line). (a) Theoretical curve is given by an I -integral that interpolates between the $k_x^{-5/3}$ to the k_x^{-1} with $a = 0.9994$ in the buffer region. (b) Theoretical curve has a uniform I -integral with the $k_x^{-5/3}$ scaling present in buffer and inertial regions.

shear stress $\tau_t > 0$. In fact for each value of the parameter β_d there is a minimum value of \tilde{y} denoted \tilde{y}_v below which $I = 0$. Only after this minimum does \tilde{y} increase with η/y . This gives the end of the viscous layer and the beginning of the buffer layer and a value of the MVP, u_v at \tilde{y}_v . It also gives the value of the fluctuation w at \tilde{y}_v and we can integrate the differential equations for u and w , with respect to y , to get the form of both functions in the buffer layer, inertial layer and the wake. Along with the formulas in the viscous layer this gives the full functional form. The differential equations use the spectral information through the full functional form of I and the two parameters β_d and β_e must be fitted to experimental data.

Approximations to the MVP and mean square fluctuations, based on the formulas in Sec. IV are given in Fig. 3 and 4, respectively. To compare with experimental data

one must solve the differential equations

$$u' = -\frac{1}{2\kappa^2 I^{3/4} y^2} + \frac{1}{\kappa I^{3/8} y} \sqrt{1 - \frac{y}{Re\sqrt{f}} + \frac{1}{4\kappa^2 I^{3/4} y^2}} \quad (49)$$

with the initial condition $u = 4.17$ at the beginning of the buffer layer $y = 4.17$. For the fluctuation we first have to solve the differential equation, ignoring term of order $O(1/y^3)$ and higher,

$$w' = \frac{\sqrt{\tau_0} - \sqrt{\langle\tau_0\rangle}}{\kappa I^{3/8} y \sqrt{\langle\tau_0\rangle}} \sqrt{1 - \frac{y}{Re\sqrt{f}}}, \quad (50)$$

with the initial condition $w = \frac{\tau_0 - \langle\tau_0\rangle}{\langle\tau_0\rangle} \left(4.17 - \frac{17.39}{2Re\sqrt{f}}\right)$, from Eq. (24), at the beginning of the buffer layer. Here $I(y)$ is the integral in Eq. (6).

In practice it is easier to vary the initial conditions than to change β_d and β_e , thus we will let the initial condition y_o , of w , from Equation (24), vary slightly depending on the Reynolds number in the simulations below. The other initial condition w_o is given by the formula $w_o = \frac{\tau_0 - \langle\tau_0\rangle}{\langle\tau_0\rangle} \left(y_o - \frac{y_o^2}{2Re\sqrt{f}}\right)$.

VII. COMPARISON WITH EXPERIMENTAL DATA

The data we use to compare with the theory comes from the wind tunnel experiments at the University of Melbourne using the nano-scale thermal anemometry probe (NSTAP) to conduct velocity measurements in the high Re number boundary layer up to $Re_\tau = 20000$. The NSTAT has a sensing length almost one order of magnitude smaller than conventional hot-wire, hence allows for a fully resolved NSTAT measurement of velocity fluctuations, [21], [1]. The size of the University of Melbourne wind tunnel and the accuracy of the NSTAT permit the measurement over a very large range of scales. We use the averaged velocity time-series at Reynolds numbers $Re_\tau = 6000, 10000, 14500, 20000$ and the averaged variance at the same Reynolds numbers. Fig. 3 shows the mean velocity profiles as a function of normalized distance from the wall, whereas Fig. 4 shows the averaged fluctuation squared (variation) as a function of the normalized distance to the wall. Both are semi-log plots.

First, let us consider the curve describing the MVP in Fig. 3 (panel b). It starts with the Eq. (23) for the viscous profile because the I -function is zero. But then we reach the value y_v where the first attached eddies appear ($y = 4.17$) and then the viscous profile changes, instead of reaching its maximum $u = Re\sqrt{f}/2$ at $y = Re\sqrt{f}$, the attached eddies increase the viscosity (decrease the Reynolds number) and the MVP reaches its maximum increase at $y \approx 15$, independent of the Reynolds number. The energy transfer of the attached eddies is captured by the I -integral and we integrate the differential equation given by Eq. (49), from $y = 4.17$, with the initial

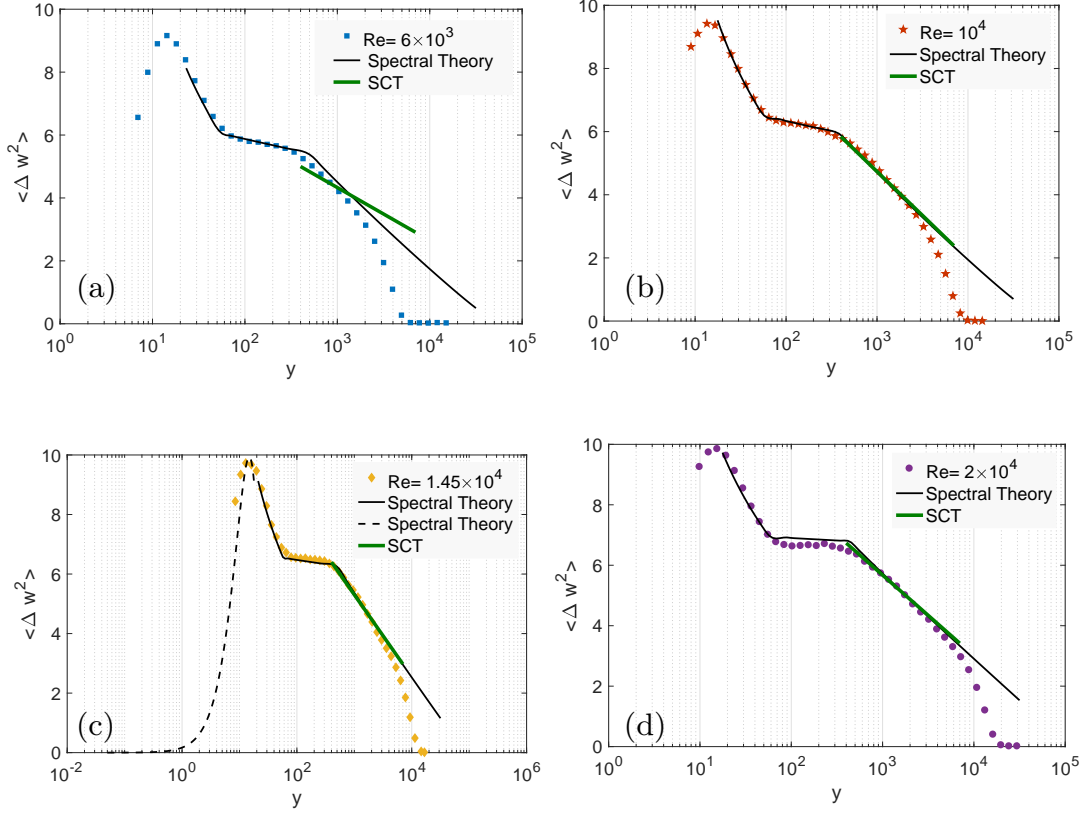


FIG. 4. The average of the fluctuation squared as a function of $\log(y)$, where y is the distance from the wall (dimensionless units). Comparison of experimental data with theory (blue line).

condition $u = 4.17$. This gives the MVP in Fig. 3 (b). This was already done in Ref. [7] and describes how the attached eddies transfer energy into the buffer and the inertial layer. However, we notice that in the predicted MVP over estimates the mean velocity in buffer region. This is because the I -function from Eq. (6) does not account for the formation of the attached eddies which reduce the net energy transfer in the direct cascade.

The curves for the fluctuations squared in Fig. 4 are obtained in a similar manner. The attached eddies fix the peak of $\langle w^2 \rangle$ at $y \approx 15$ and the peak profiles can be fitted by the viscous formula $\langle w^2 \rangle = a(y - \frac{y^2}{30})^2$ where $a \sim (\langle \tau_o^2 \rangle - \langle \tau_o \rangle^2) / \langle \tau_o \rangle^2$. This fit is shown in Fig. 4 (c). The peak position is experimentally observed to be fixed, but its height shows a weak Reynolds number dependence $a = -3.06 + 0.99 \log(Re)$, see [21]. This relationship can be tested using our theory and this will be done in another publication, see also [5]. Then, we integrate the differential equation from Eq. (50) for w with the initial data described in last section from some point to the right of the peak, where above peak profile fits the initial condition, this give the profile of the fluctuations squared down to the flat part in the buffer layer. At the beginning of the flat part, $y \approx 60$, the second scaling from Section

II begins to dominate the fluctuations, modeling an inverse cascade of attached eddies in the buffer layer. Then we switch to the buffer I -function I_b in the integration and integrate with I_b until we get into the inertial region where the Kolmogorov-Obukhov scaling dominates again and the attached eddies break up. This produces the curves in Fig. 4.

We can now compare the functional form of the fluctuations squared shown in Fig. 4 with the predictions of the stochastic closure theory (SCT) of turbulence, used in Refs. [4] and [12], to compute the Townsend-Perry constants, in the inertial (log) layer. These computations use the first structure function S_1 of turbulence and we explain how they are performed, see [4] and [12] for more information. The computed Townsend-Perry constants are listed in Table I.

The first structure function of turbulence is, see [11],

$$E(|u(x, t) - u(y, t)|) = S_1(x, y, t) = \frac{2}{C} \sum_{k \in \mathbb{Z}^3 \setminus \{0\}} \frac{|d_k| (1 - e^{-\lambda_k t})}{|k|^{\zeta_1 + \frac{4\pi^2\nu}{C}} |k|^{\zeta_1 + \frac{4}{3}}} |\sin(\pi k \cdot (x - y))|,$$

where the Reynolds number dependence enters through the viscosity ν , and E denotes the expectation (ensemble)

| Re_λ | C_1 | A_1 | B_1 |
|--------------|--------|-------|--------|
| 6000 | 9.449 | 0.730 | 9.373 |
| 10,000 | 15.628 | 1.207 | 13.073 |
| 14,500 | 15.500 | 1.197 | 13.573 |
| 20,000 | 14.994 | 1.158 | 13.673 |

TABLE I. Here, the approximate A_1 value is computed from C_1 using the proportionality factor $A_1 = C_1/(K|y^*|^{\zeta_1}) = C_1/12.952$.

average). To get the Kolmogorov-Obukhov coefficients, C_p in

$$S_p(r, \infty) \sim C_p r^{\zeta_p}, \quad (51)$$

for the lag variable r small, and ζ_p the scaling exponents, we send t to ∞ in the above formulas and project onto the longitudinal lag variable $\mathbf{r} = (r, 0, 0)$. For $p = 1$ this becomes

$$\begin{aligned} S_1 &\sim \frac{2\pi\zeta_1}{C} \sum_{k \neq 0} \frac{|d_k|}{(1 + \frac{4\pi^2\nu}{C}|k|^{4/3})} r^{\zeta_1} \\ &= \frac{4\pi\zeta_1}{C} \sum_{k=1}^{\infty} \frac{a}{(a^2 + k^m)(1 + \frac{4\pi^2\nu}{C}|k|^{4/3})} r^{\zeta_1}, \end{aligned} \quad (52)$$

see [11], where $\zeta_1 = 0.37$, see [2]. Now we use the values for ν in Table 1 in [12], and the corresponding values for a , m and C from Table 3 in the same paper. The Reynolds numbers, 6430, 10,770, 15,740 and 19,670 are close enough to ours 6000, 10,000, 14,500, and 20,000, that we can use value of the parameters in [12]. This gives the values in Table I, where $A_1 \sim K|y^*|^{\zeta_1} C_1$, see Section V, and the proportionality factor $K|y^*|^{\zeta_1} = 1/12.952$ is computed at the Reynolds number 15,470, where the approximated A_1 coincides with the measured A_1 . The log functions with coefficient A_1 , from the third column in Table I, and using the constant B_1 from the fourth column in Table I, are then compared to the experimental and theoretical values in Fig. 4. The spanwise Townsend-Perry constants, for the spanwise fluctuations, can computed similarly by projecting onto the spanwise lag variable $\mathbf{t} = (0, t, 0)$.

In Fig. 4 panel (a), the Townsend-Perry constant A_1 computed by the SCT does not agree with the measured slope. This was already observed in Ref. [12], since for low Reynolds numbers the C_1 s do not provide a good approximation to the A_1 s. They only do for large Reynolds numbers and the discrepancy (a) occurs at the smallest Reynolds number. This does not happen for the Generalized Townsend-Perry constants, the reasons are explained in Ref. [12], and for them the C_p s, $p \geq 2$, provide good approximations to the A_p s for all Reynolds numbers.

VIII. DISCUSSION

We used the spectral theory of the MVP and the variation profile to represent both, and compare with exper-

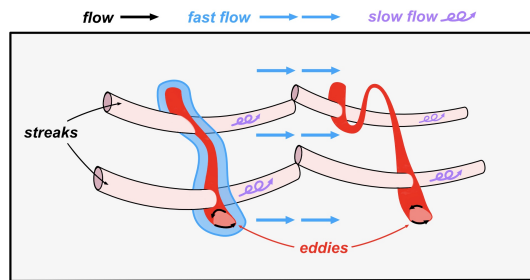


FIG. 5. Sketch of the instantaneous streaks, in the stream-wise direction, and the wall-attached eddies, in the spanwise direction.

iment [21] for a range of Reynolds numbers. Assuming that the wall shear stress is a fluctuating quantity, we can derive that log-law for the variation (2) that was proposed by Townsend and measured by Perry and Chong. This law involves the Townsend-Perry constants. This was first done in the large Reynolds number limit and then for general Reynolds numbers. The Reynolds number dependence of the Townsend-Perry constants is determined by the stochastic closure theory [4], [12]. We derive the log-law for the higher moments of the fluctuations and the Generalized Townsend-Perry constants based on the functional form of the variation and use the stochastic closure theory to express them in terms of the Kolmogorov-Obukhov coefficients of the structure functions of turbulence [11]. This confirms the results in Refs. [4] and [12].

The spectral function I derived in Ref. [7] plays a central role in this theory. It can be considered be the analytic expression of Townsend's theory of wall-attached eddies. It quantifies when the first eddies appear at the boundary of the viscous and the buffer layer and when they are fully developed in the inertial layer. It even quantifies the limit of their influence in the energetic wake. By introducing the spectral theory into the analysis it resolves many of the issues that we are faced with in boundary layer turbulence.

The I -function corresponds to the Kolmogorov-Obukhov cascade $k_x^{-5/3}$ in the inertial layer, but in the buffer layer another cascade k_x^{-1} dominates the fluctuations, although its influence on the MVP is small. This is an inverse cascade that can accelerate larger and larger attached eddies. The energy transfer of this cascade is captured by the I -function in buffer layer, I_b . With it we are able to produce the functional form of the averaged fluctuations square in the buffer layer. Once in the inertial layer the original I -function dominates again.

The final confirmation of this spectral theory is how we are able to improve the fit to experimental values of the MVP in Ref. [7], by use of the I_b function in the buffer layer. Although, this effect on the MVP is small, the attached eddies, siphon a small amount of energy from the MVP in the buffer layer. We model this by linear combination of the I and I_b function $(1-a)I + aI_b$,

in the buffer layer, where a is small. This produces a better fit to the measured MVP in the buffer region as shown in Figure 3 (a), whereas the fit without this linear combination, shown in Figure 3 (b), is not as good.

It is fair to ask what the Townsend attached eddies actually look like since our spectral method is based on them. Unlike the streamwise streaks and associated vortices that have been visualized since the experiments of Kline et al. in the 1960s, see Refs. [13] and [10], the attached eddies are difficult to visualize, either in experiments or simulations. We provide a sketch in Fig. 5, where streamwise streaks are visualized gradually lifting from the boundary by the flow, and perpendicular to them are spanwise attached eddies being deformed by the alternating slow and fast streamwise flow into a hair-

pin vortex. This does happen both in experiments and observations, see Ref. [16]. However, these hairpin vortices are made unstable by the striations in the streamwise flow and the typical attached eddies are irregular in shape, with the general feature of being stretched by the flow and attached to the wall. One must interpret their influence in a statistical sense.

Acknowledgements: We are thankful to Ivan Marusic, Milad Samie and Christian E. Willert for kindly sharing with us the wind turbulence experimental data, and Joe Klewicki for useful conversations. We are grateful to Knut Bauer for proving us with the graphic illustrations. This research was supported in part by the National Science Foundation under Grant No. NSF PHY-1748958 through the Kavli Institute for Theoretical Physics.

-
- [1] Rio Baidya, WJ Baars, Spencer Zimmerman, Milad Samie, R Jason Hearst, Eda Dogan, Lucia Mascotelli, X Zheng, Gabriele Bellani, A Talamelli, et al. Simultaneous skin friction and velocity measurements in high reynolds number pipe and boundary layer flows. *Journal of Fluid Mechanics*, 871:377–400, 2019.
 - [2] B. Birnir. The Kolmogorov-Obukhov statistical theory of turbulence. *J. Nonlinear Sci.*, 2013. DOI 10.1007/s00332-012-9164-z.
 - [3] B. Birnir. *The Kolmogorov-Obukhov Theory of Turbulence*. Springer, New York, 2013.
 - [4] B. Birnir and X. Chen. Sub-gaussian behavior of the Townsend-Perry constants in turbulent boundary layers. *Physical Review E*, 93(1):011101, 2016.
 - [5] X. Chen and K. R. Sreenivasan. Reynolds number scaling of the peak turbulence intensity near the wall. *Submitted to Journal of Fluid Mechanics*, 2020.
 - [6] Xi Chen, Fazle Hussain, and Zhen-Su She. Non-universal scaling transition of momentum cascade in wall turbulence. *Journal of Fluid Mechanics*, 871, 2019.
 - [7] G. Gioia, N. Guttenberg, N. Goldenfeld, and P. Chakraborty. Spectral theory of the turbulent mean-velocity profile. *Physical Review Letters*, 105, 2010.
 - [8] Gustavo Gioia and Pinaki Chakraborty. Turbulent friction in rough pipes and the energy spectrum of the phenomenological theory. *Physical Review Letters*, 96(4):044502, 2006.
 - [9] Javier Jiménez. Near-wall turbulence. *Physics of Fluids*, 25(10):101302, 2013.
 - [10] Javier Jiménez and Alfredo Pinelli. The autonomous cycle of near-wall turbulence. *Journal of Fluid Mechanics*, 389:335–359, 1999.
 - [11] J. Kaminsky, B. Birnir, G. Bewley, and M. Sinhuber. Reynolds number dependence of the structure functions in homogeneous turbulence. *Journ. of Nonlin. Sci.*, pages 1–34, 2020.
 - [12] J. Kaminsky, B. Birnir, and J. Klewicki. The application of the stochastic closure theory to the generalized Townsend-Perry constants. *Phys. Rev. E, Rapid Communications*, 100(6):061101, 2019.
 - [13] Stephen J Kline, William C Reynolds, FA Schraub, and PW Runstadler. The structure of turbulent boundary layers. *Journal of Fluid Mechanics*, 30(4):741–773, 1967.
 - [14] M Lee and RD Moser. Dns of turbulent channel flow up to $re_\tau \approx 5200$. *J. Fluid Mech.*, 774:395–415, 2015.
 - [15] I. Marusic and C. Meneveau. Generalized logarithmic law for high-order moments in turbulent boundary layers. *J. Fluid Mech.*, 719, R1:1–11, 2013.
 - [16] Ivan Marusic and Jason P Monty. Attached eddy model of wall turbulence. *Annual Review of Fluid Mechanics*, 51:49–74, 2019.
 - [17] Martin Oberlack. Self-similar mean velocity profiles in plane parallel turbulent shear flows. 1997.
 - [18] A E Perry and M S Chong. *Journal of Fluid Mechanics*, 119, 1982.
 - [19] A E Perry and et al. *Journal of Fluid Mechanics*, 165, 1986.
 - [20] Ludwig Prandtl. Essentials of fluid dynamics: with applications to hydraulics, aeronautics, meteorology and other subjects. 1953.
 - [21] M Samie, I Marusic, N Hutchins, MK Fu, Y Fan, M Hultmark, and AJ Smits. Fully resolved measurements of turbulent boundary layer flows up to $Re_\tau = 20\,000$. *Journal of Fluid Mechanics*, 851:391–415, 2018.
 - [22] Alexander J Smits and Ivan Marusic. Wall-bounded turbulence. *Phys. Today*, 66(9):25–30, 2013.
 - [23] Federico Toschi and Eberhard Bodenschatz. Lagrangian properties of particles in turbulence. *Annual review of fluid mechanics*, 41:375–404, 2009.
 - [24] A. A. Townsend. *The Structure of Turbulent Shear Flow*. Cambridge University Press, 1976.
 - [25] JC Vassilicos, J-P Laval, J-M Foucaut, and Michel Stanislas. The streamwise turbulence intensity in the intermediate layer of turbulent pipe flow. *Journal of Fluid Mechanics*, 774:324–341, 2015.
 - [26] WF Vinen and JJ Niemela. Quantum turbulence. *Journal of Low Temperature Physics*, 128(5-6):167–231, 2002.
 - [27] John C Wyngaard. Atmospheric turbulence. *Annual Review of Fluid Mechanics*, 24(1):205–234, 1992.